

Microslips as precursors of large slip events in the stick-slip dynamics of sheared granular layers: A discrete element model analysis

B. Ferdowsi,^{1,2} M. Griffa,² R. A. Guyer,^{3,4} P. A. Johnson,³ C. Marone,⁵ and J. Carmeliet^{2,6}

Received 24 June 2013; accepted 31 July 2013.

[1] We investigate the stick-slip behavior of a granular system confined and sheared by deformable solid blocks using three-dimensional discrete element method simulations. Our modeling results show that large slip events are preceded by a sequence of small slip events—microslips—whose occurrence accelerates exponentially before the large slip event onset. Microslips exhibit energy release several orders of magnitude smaller than the large slip events. The microslip event rate is proposed as a measure of slip activity in the granular gouge layer. A statistical analysis shows that microslip event rate correlates well with large slip event onset and that variations in it can be used to predict large slip events. The emergence of microslips and their duration are found to be controlled by the value of the slipping contact ratio and are therefore related to the jamming/unjamming transition of frictional granular packings. **Citation:** Ferdowsi, B., M. Griffa, R. A. Guyer, P. A. Johnson, C. Marone, and J. Carmeliet (2013), Microslips as precursors of large slip events in the stick-slip dynamics of sheared granular layers: A discrete element model analysis, *Geophys. Res. Lett.*, 40, doi:10.1002/grl.50813.

1. Introduction

[2] Tectonic fault zones contain granular media known as fault gouge. Fault gouge plays a fundamental role in determining the fault's frictional strength and the earthquake slip dynamics. Fault systems accumulate strain energy during the interseismic period of the seismic cycle, just as a sheared granular layer does during the “stick” phase of the stick-slip cycle [Brace and Byerlee, 1966; Johnson et al., 1973]. Understanding and characterizing the behavior of sheared granular layers in numerical simulations and laboratory studies can provide important insight into the influence of microscopic physics of granular friction on faults' behavior.

[3] There is increasing evidence that some proportion of large earthquakes are preceded by a period of accelerating slip activity of small- to moderate-sized earthquakes, foreshocks, or slow slip events [Sykes and Jaume, 1990; Kato et al., 2012; Bouchon et al., 2012, 2013]. These observations are in agreement with a scenario where foreshocks are the manifestation of an initiation process leading to the main shock [Ohnaka, 1993; Abercrombie and Mori, 1996]. At the fault gouge scale, stick-slip experiments show that slow displacements occur prior to the onset of large and rapid slip events, such that there is a transition from quasi-static creep to rapid and dynamic slip, e.g., Marone [1998] and Nasuno et al. [1997] for sheared granular gouge layers, and Rubinstein et al. [2007] and Baumberger et al. [1994] for solid-on-solid frictional interaction. The slow creep-like displacements can be explained by the occurrence of microslips and microfailures in the system [Amon et al., 2013; Pica Ciamarra et al., 2010; Papanikolaou et al., 2012]. Microslips drive the granular system to a local energy minimum, while large slip events accompany a large amount of energy release and correspond to a significant reorganization of the granular assembly itself, in terms of contacts and contact forces [Pica Ciamarra et al., 2010].

[4] In this paper, the stick-slip behavior of a sheared fault gouge is simulated by the 3-D discrete element method (DEM) [Cundall and Strack, 1979; Place and Mora, 1999; Wang et al., 2006]. We report a detailed investigation of microslip occurrence, their grain-scale mechanisms, and their relation to energy release during granular shearing and large slip events.

2. Model

[5] Figure 1a illustrates the simulated granular gouge layer. The model consists of three layers of particles: a driving block at the top, a granular gouge layer, and a substrate block at the bottom. The driving and substrate blocks are used to confine the granular gouge by applying a constant normal force in the Y direction. The top driving block moves at constant velocity in the positive X direction and applies a shear force to the granular gouge layer. Each variable/parameter in our 3-D DEM model is expressed in terms of the following basic dimensional units: $L_0 = 150 \mu\text{m}$, $t_0 = 1 \text{ s}$, and $M_0 = 1 \text{ kg}$, for length, time, and mass, respectively. We run sheared granular layer simulations at a confining pressure of $\sigma_n = 40 \text{ MPa}$ and shearing velocity of $V_{X,0} = 0.004 \frac{L_0}{t_0}$ to achieve stick-slip dynamics. Further details about the model are provided in the supporting information.

3. Results

[6] The stick-slip behavior of the granular gouge layer is monitored by friction coefficient time series. The fric-

Additional supporting information may be found in the online version of this article.

¹Department of Civil, Environmental and Geomatic Engineering, Swiss Federal Institute of Technology Zürich, Zürich, Switzerland.

²Swiss Federal Laboratories for Materials Science and Technology, Empa, ETH Domain, Dübendorf, Switzerland.

³Solid Earth Geophysics Group, Los Alamos National Laboratory, Los Alamos, New Mexico, USA.

⁴Department of Physics, University of Nevada, Reno, Nevada, USA.

⁵Department of Geosciences and G3 Center and Energy Institute, Pennsylvania State University, University Park, Pennsylvania, USA.

⁶Chair of Building Physics, Swiss Federal Institute of Technology Zürich, Zürich, Switzerland.

Corresponding author: B. Ferdowsi, Department of Civil, Environmental and Geomatic Engineering, Swiss Federal Institute of Technology Zürich, Zürich, Switzerland. (behrooz.ferdowsi@empa.ch; behroozf@ethz.ch)

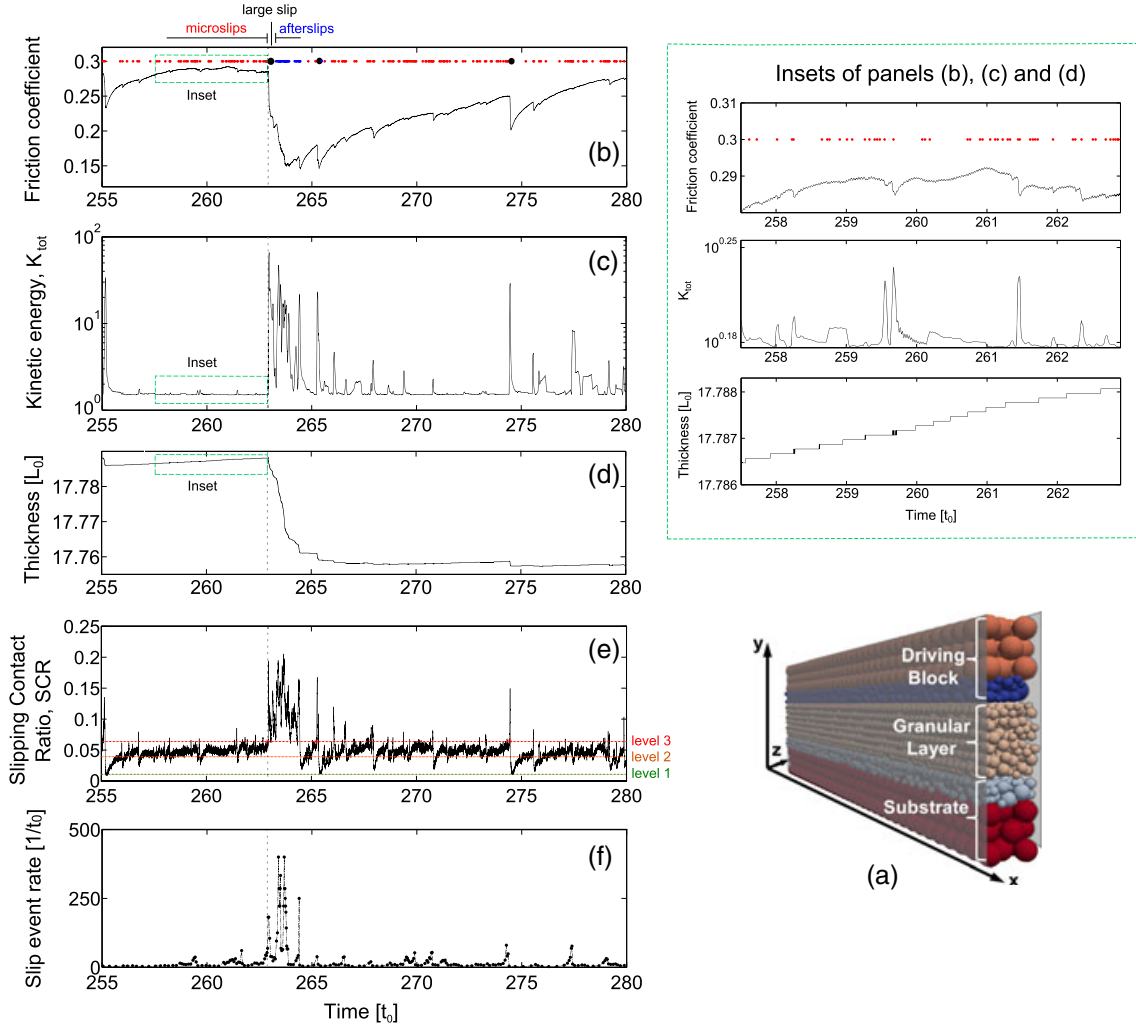


Figure 1. (a) 3-D DEM model comprised of (top) the driving block, (middle) a granular gouge layer, and (bottom) a substrate block. (b) Friction coefficient time series of a stick-slip event. Inset shows the same time series for the time interval $[257.5; 262.9]t_0$. (c) Total kinetic energy, K_{tot} , time series. Inset shows the same time series for the time interval $[257.5; 262.9]t_0$. (d) Thickness of the granular layer. (e) Slipping contact ratio, SCR, time series. (f) Slip event rate, SER, time series. The vertical dashed lines in different panels show onset of the large event at $t \approx 263[t_0]$.

tion coefficient, μ , is defined as the ratio of shear stress developed at the boundary layers to the imposed normal stress. In the following, we focus on a large slip event and associated activity that takes place prior to this event. Figure 1b shows a characteristic time series of the friction coefficient for the time interval $[255; 280]t_0$. Slip events are identified when the first-order derivative of the friction coefficient becomes negative and lower than a threshold equal to $-3 \times 10^{-2}t_0^{-1}$. This threshold is chosen to be small enough to capture small events, but large enough to avoid capturing the intrinsic fluctuations of the friction coefficient due to the granular dynamics (By “granular dynamics,” we mean slow rearrangement of particles due to constant shear velocity applied to the top boundary of the granular layer. These small rearrangements of particles are always present in the friction coefficient signal as a background fluctuation.) In Figure 1b, a characteristic large slip event occurs at $t_1 \approx 263[t_0]$. Figure 1c shows the time series of the granular layer’s total kinetic energy, which is the energy due to particles movement (complete definition is provided in the supporting information). We distinguish three primary

categories of slip events: large slips, microslips before a large slip (red symbols, Figure 1b) and afterslips that follow the large slip event (blue symbols, Figure 1b). The distinction between the three types of slip events is based on the change in the granular layer’s total kinetic energy during the slip event. At the onset of a slip event, the kinetic energy increases sharply from the background level. The largest energy release, which results from the elastic potential energy stored in particle contacts, occurs at the moment of a large slip event. A detailed look at the friction coefficient and kinetic energy before the large event at $t_1 \approx 263[t_0]$ is given in the insets. We observe that many small slip events manifest by abrupt increases of kinetic energy compared to the background level. These slip events release between 1 and 6 orders of magnitude smaller energy compared to the large slip event. If an event is large enough (like at $t_1 \approx 263[t_0]$) to activate other susceptible jammed regions of the granular layer, we observe afterslips closely clustered in time after the large event. During afterslips, the kinetic energy signal is elevated above the background level preceding the large event, and afterslips involve an energy

release comparable to the large slip event. Figure 1d shows the thickness of the granular layer. At the time of the large slip event, the thickness of the granular gouge layer shows a drastic compaction (thickness reduction). Microslips occur in association with dilation of the granular gouge during the stick phase (inset). The grain rearrangements can be characterized by study of the slipping contacts [Aharonov and Sparks, 2004]. The ratio of the number of slipping contacts, i.e., those contacts in which the tangential contact force is at the Coulomb threshold, to the total number of contacts is called Slipping Contact Ratio (SCR) and is presented in Figure 1e. We distinguish three levels of the SCR during the stick phase of a characteristic large event. At the beginning of the stick phase, the SCR is about 0.01 (level 1) and no microslips occur at this stage. As the friction coefficient increases, the shear force between the particles increases; hence, the SCR increases until it reaches a value of about 0.04 (level 2). From this level on, the SCR slightly and gradually increases, and microslips appear with an increasing frequency until the SCR reaches a value of about 0.06 (level 3) where the large slip event occurs. The afterslips cluster after the large event where the SCR is still higher than level 3. The large values for the SCR during afterslips explain why their energy release differs noticeably from microslips.

[7] We use the Slip Event Rate (SER), defined as the number of slip events per time unit as a measure of slip activity. The SER includes microslips, large slip events, and afterslips without distinguishing between them. Figure 1f shows the slip event rate for the time interval $[255; 280]t_0$. We observe that the large slip event coincides with a noticeable increase in the slip event rate.

[8] So far, we have presented one characteristic large event in our model, its properties, and the event activity that takes place before and after its occurrence. We next investigate the microslip activity that precedes large slip events with different slip event size. The size of a slip event is measured in terms of its total energy release, E . The definition of E is explained in the supporting information. In order to compare slip events with different time scales, we use a normalized time (to failure) as described in Figure 2a. $t_{\text{norm}} = -1$ corresponds to the beginning of the stick phase of a specific slip event, while $t_{\text{norm}} = 0$ corresponds to when the slip/failure happens. Figure 2b shows the probability of microslips occurrence during the stick phase of slip events with different event size ranges. The plot summarizes the results for a total of 44,000 slip events taking place during a long simulation interval, $H = [200; 8000]t_0$. Figure 2b indicates that microslips occur randomly during the stick phase. However, their occurrence accelerates exponentially close to the event onset ($-0.02 < t_{\text{normalized}} < 0.0$) for events with size $E > 1.0 \times 10^{-6} M_0 \cdot L_0^2 \cdot t_0^{-2}$. The nonlinear acceleration of microslips occurrence exists less significantly for events with $1.0 \times 10^{-7} < E < 1.0 \times 10^{-6} M_0 \cdot L_0^2 \cdot t_0^{-2}$, and it disappears for smaller events. We therefore call those events with $E > E_{\text{thresh}} = 1.0 \times 10^{-6} M_0 \cdot L_0^2 \cdot t_0^{-2}$ as “large” events. The events occurring at $t_1 \approx 263[t_0]$, $t_2 \approx 265.2[t_0]$, and $t_3 \approx 274.5[t_0]$ shown with black markers in Figure 1a are examples of large events in our model. We choose to explore the precursory behavior for these “large” events.

[9] Figure 2c shows the complementary Cumulative Distribution Function (cCDF) of the energy release, E , for a total of 898 large slip events during the interval H . The

distribution follows a power law (for $E > 1.0 \times 10^{-6}$), $\text{cCDF}(E) \propto E^{-\beta}$ with $\beta \simeq 1.23$.

[10] Having confirmed the exponential acceleration of microslips occurrence before large slip events, we perform a pairwise sliding window cross-correlation analysis for the time series of the event energy release $E(t)$ and slip event rate, $\text{SER}(t)$. This is to statistically evaluate whether or not the increase in SER can be used as a further indicator (precursor) for a large slip event. After calculating the cross-correlation coefficient $\rho(t)$ as a function of time, we determine for each large slip event the maximum cross-correlation coefficient, ρ_{max} , and the time lag between the instant when the cross-correlation is maximal and the onset of the large slip event, τ_{max} . An example of the events energy and SER time series as well as cross-correlation results for those time series are provided in the supporting information. A high cross-correlation coefficient $\rho_{\text{max}} (> 0.8)$ and negative time lag means that on average, microslips anticipate a large slip event. The distributions of ρ_{max} and τ_{max} considering all large slip events ($E > E_{\text{thresh}}$) are plotted in Figures 2d and 2e, respectively. The average maximal cross-correlation coefficient is 0.8187, and the average time lag is $-0.0525[t_0]$. More than 85% of large slip events have a cross-correlation coefficient higher than 0.75. About 75% of large slip events have negative time lags. The remaining 25% of large slip events have zero time lags. The zero time lags are mainly due to those events whose afterslip activity masks the precursory microslips. It is also partially due to the resolution of the cross-correlation analysis and the running average used for smoothing the SER and the energy release time series.

4. Discussion

[11] The observation of microslips in our numerical simulation is in agreement with laboratory and theoretical studies which suggest that earthquakes are preceded by a nucleation process where quasi-static creep develops into dynamically driven motion within a confined zone on a fault [Dieterich, 1978; Marone, 1998; Kawamura et al., 2012]. Precursory activities in the form of creep deformation and aseismic slips have also been reported for large earthquakes worldwide [Ellsworth and Beroza, 1995; Peng and Gomberg, 2010]. The most recent and profound example is the evidence of small repeating earthquakes that led to the 2011 moment magnitude M_w 9.0 Tohoku-Oki event [Kato et al., 2012; Bouchon et al., 2012]. There also exist evidences of similarities between microslip phenomena and slow slip events (Episodic Tremor and Slip, ETS) observed on the deeper interface of the northern Cascadia subduction zone [Garry and Dragert, 2003]: ETS events are several orders of magnitude smaller than regular earthquakes in terms of stress drop and energy release [Vidale and Houston, 2012]. In addition, a majority of ETS events occur in the dilatational quadrants of the strain field on both sides of the plate interface [Kao et al., 2006]. Similarly, in our DEM model, microslips energy release are orders of magnitude smaller than large slips, and they occur during dilatant strengthening of the granular gouge layer. It is suggested that pore pressure can be a competing mechanism with dilation for further occurrence of either slow or fast slip in the course of ETS activities [Segall et al., 2010]. Development of a fluid coupled DEM model can provide insight on the pore pressure evolution during microslips.

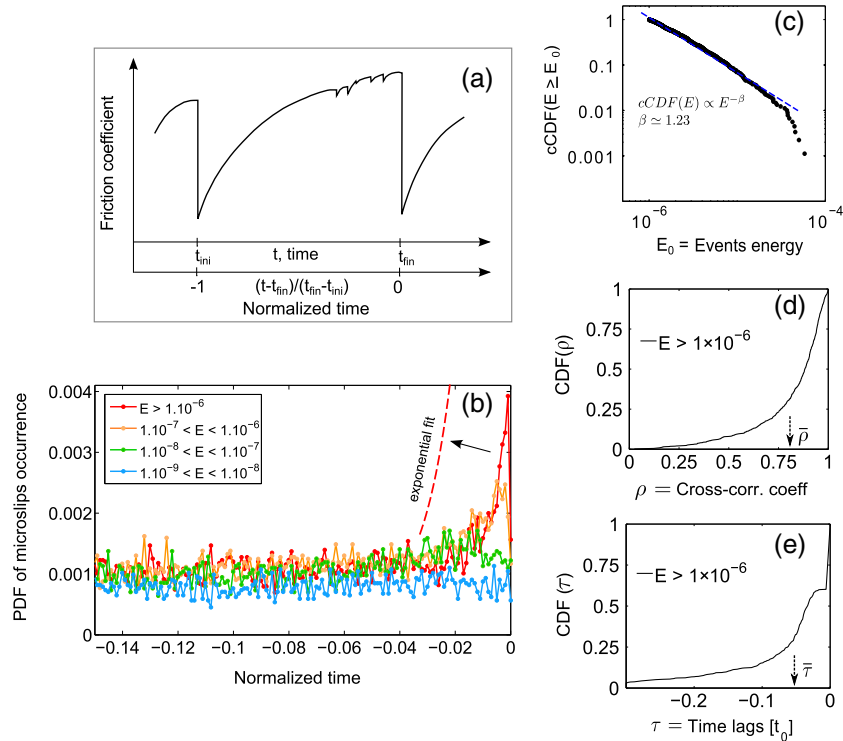


Figure 2. (a) A schematic slip event with normalized time scale. (b) Probability of microslip occurrence for a range of events sizes as noted. (c) Distribution (cCDF) of large slip event energy size for the time interval H (see text). (d) Distribution of cross-correlation coefficient values for the time series of $E(t)$ and $SER(t)$. (e) Distribution of time lag values (see text for explanation). Arrows in Figures 2d and 2e show the average values.

[12] Our numerical observations reveal that microslips occurrence accelerates exponentially for events designated “large” based on their energy release. A similar pattern of nonlinear acceleration of precursory activity has been observed in experimental stick slip in sheared granular layers by *Nasuno et al.* [1997] and in large interplate earthquakes worldwide by *Bouchon et al.* [2013]. The precursory activity becomes less important and significant for smaller event size. Statistical analysis of SER and slip events energy release further confirms the occurrence of precursory activity of microslips before large slip events. SER might be a better measure in this sense since we do not distinguish between different event size in forming its time series.

[13] The evolution of the SCR (Slipping Contact Ratio) during a characteristic stick phase implies that a background level of slipping contacts always exists in a dense sheared granular layer and plays a major role in slow rearrangement of particles and loss/formation of old/new contacts. Microslips start to appear only when the SCR rises above a certain minimum level. Further increase of the SCR above a certain level results in an increase of SER, which leads to the onset of a large slip event. The critical SCR value controls the lower bound of the isostatic coordination number for frictional packings; therefore, its increase forces the medium from a marginally (shear-) jammed to unjammed state [*Shundyak et al.*, 2007; *Song et al.*, 2008; *Bi et al.*, 2011]. This also hints that the controlling parameters of minimum and critical slipping ratio values (grain-scale friction, particle packing, particle size distribution, shearing velocity, and confining pressure) are among the parameters which

influence the duration and intensity of microslips occurrence. The analysis of the microslips, e.g., by investigating the development of affine and nonaffine deformations in the granular gouge layer during microslips [*Griffa et al.*, 2011, 2012] may allow us to further characterize how the microslips signal the approaching of a large slip event.

[14] The distribution of large slip events in our model follows a power law with $\beta \simeq 1.23$. The β value complies with observationally found values for earthquakes [*Kanamori and Anderson*, 1975; *Kagan*, 1991; *Godano and Pingue*, 2001]. The observed scaling is also in agreement with the avalanche experiments of microslips and nanosized crystals [*Dimiduk et al.*, 2006; *Friedman et al.*, 2012; *Papanikolaou et al.*, 2012].

5. Conclusions

[15] We have presented the results of 3-D DEM modeling of a sheared granular gouge layer in the stick-slip regime. We show that there is precursory activity due to the occurrence of small slip events, called microslips, that precede the onset of large slip events. Microslips occurrence accelerates exponentially shortly before the onset of large slip events. The slip event rate is examined as a more rigorous measure that shows significant increase when approaching a large slip event. The increase is particularly accentuated before the large slip onset. The onset and duration of microslips emergence are controlled by the slipping contact ratio in the granular layer which connects the precursory microslips to the jamming-unjamming transition of the granular layer. The results of this study allow us to advance our understanding

of the earthquake initiation on mature faults and to develop analysis methods to be used in seismology for improving probabilistic hazard assessment.

[16] **Acknowledgments.** We thank D. Weatherley and S. Abe for support for the ESyS-Particle code and D. Passerone and C. Pignedoli for the help with the computational cluster of Empa, Ipazia. Our work has been supported by the Swiss National Science Foundation (projects 206021-128754 and 200021-135492) and by the LDRD Program (Institutional Support) at the Los Alamos National Laboratory, Department of Energy, USA.

[17] The Editor thanks Karen Mair for her assistance in evaluating this paper.

References

- Abercrombie, R. E., and J. Mori (1996), Occurrence patterns of foreshocks to large earthquakes in the Western United States, *Nature*, *381*, 303–307.
- Aharonov, E., and D. Sparks (2004), Stick-slip motion in simulated granular layers, *J. Geophys. Res.*, *109*, B09306, doi:10.1029/2003JB002597.
- Amon, A., R. Bertoni, and J. Crassous (2013), Experimental investigation of plastic deformations before granular avalanche, *Phys. Rev. E*, *87*, 012204.
- Baumberger, T., F. Heslot, and B. Perrin (1994), Crossover from creep to inertial motion in friction dynamics, *Nature*, *367*, 544.
- Bi, D., J. Zhang, B. Chakraborty, and R. P. Behringer (2011), Jamming by shear, *Nature*, *480*, 355–358.
- Bouchon, M., H. Karabulut, M. Aktar, C. Özalaybey, J. Schmittbuhl, and M.-P. Bouin (2012), Extended nucleation of the 1999 M_w 7.6 Izmit earthquake, *Science*, *331*, 877.
- Bouchon, M., V. Durand, D. Marsan, H. Karabulut, and J. Schmittbuhl (2013), The long precursory phase of most large interplate earthquakes, *Nat. Geosci.*, *6*, 1769–1785.
- Brace, W. F., and J. D. Byerlee (1966), Stick-slip as a mechanism for earthquakes, *Science*, *153*, 990–992.
- Cundall, P. A., and O. D. L. Strack (1979), A discrete numerical model for granular assemblies, *Geotechnique*, *29*, 47–65.
- Dieterich, J. H. (1978), Time-dependent friction and the mechanics of stick-slip, *Pure Appl. Geophys.*, *116*, 790–806.
- Dimiduk, D. M., C. Woodward, R. LeSar, and M. D. Uchic (2006), Scale-free intermittent flow in crystal plasticity, *Science*, *312*, 1180–1190.
- Ellsworth, W. L., and G. C. Beroza (1995), Seismic evidence for an earthquake nucleation phase, *Science*, *268*, 851–855.
- Friedman, N., A. T. Jennings, G. Tsekenis, J. Y. Kim, M. Tao, J. T. Uhl, J. R. Greer, and K. A. Dahmen (2012), Statistics of dislocation slip avalanches in nanosized single crystals show tuned critical behavior predicted by a simple mean field model, *Phys. Rev. Lett.*, *109*, 095507.
- Garry, R., and H. Dragert (2003), Episodic tremor and slip on the Cascadia subduction zone: The chatter of silent slip, *Science*, *300*, 1942–1943.
- Godano, C., and F. Pingue (2001), Is the seismic moment-frequency relation universal?, *Geophys. J. Int.*, *142*, 193–198.
- Griffa, M., E. G. Daub, R. A. Guyer, P. A. Johnson, C. Marone, and J. Carmeliet (2011), Vibration-induced slip in sheared granular layers and the micromechanics of dynamic earthquake triggering, *Europhys. Lett.*, *96*, 14001.
- Griffa, M., B. Ferdowsi, E. G. Daub, R. A. Guyer, P. A. Johnson, C. Marone, and J. Carmeliet (2012), Meso-mechanical analysis of deformation characteristics for dynamically triggered slip in a granular medium, *Philos. Mag.*, *92*, 3520–3539.
- Johnson, T., F. T. Wu, C. H. Scholz, and S. Uri (1973), Source parameters for stick-slip and for earthquakes, *Science*, *179*, 278–280.
- Kagan, A. A. (1991), Seismic moment distribution, *Geophys. J. Int.*, *106*, 123–134.
- Kao, H., S.-J. Shan, H. Dragert, G. Rogers, J. F. Cassidy, K. Wang, T. S. James, and K. Ramachandran (2006), Spatial-temporal patterns of seismic tremors in northern Cascadia, *J. Geophys. Res.*, *111*, B03309, doi:10.1029/2005JB003727.
- Kanamori, H., and D. L. Anderson (1975), Theoretical basis of some empirical relations in seismology, *Bull. Seismol. Soc. Am.*, *65*, 1073–1095.
- Kato, A., K. Obara, T. Igarashi, H. Tsuruoka, S. Nakagawa, and N. Hirata (2012), Propagation of slow slip leading up to the 2011 M_w 9.0 Tohoku-Oki earthquake, *Science*, *335*, 705–708.
- Kawamura, H., A. Hatano, N. Kato, S. Biswas, and B. K. Chakrabarti (2012), Statistical physics of fracture, friction, and earthquakes, *Rev. Mod. Phys.*, *84*, 839–834.
- Marone, C. (1998), Laboratory-derived friction laws and their application to seismic faulting, *Annu. Rev. Earth Planet. Sci.*, *26*, 643–696.
- Nasuno, S., A. Kudrolli, and J. P. Gollub (1997), Friction in granular layers: Hysteresis and precursors, *Phys. Rev. Lett.*, *79*, 949–952.
- Ohnaka, M. (1993), Critical size of the nucleation zone of earthquake rupture inferred from immediate foreshock activity, *J. Phys. Earth*, *41*, 45–46.
- Papanikolaou, S., D. M. Dimiduk, W. Choi, J. P. Sethna, M. D. Uchic, C. F. Woodward, and S. Zapperi (2012), Quasi-periodic events in crystal plasticity and the self-organized avalanche oscillator, *Nature*, *490*, 517–521.
- Peng, Z., and J. Gombert (2010), An integrated perspective of the continuum between earthquakes and slow-slip phenomena, *Nat. Geosci.*, *3*, 599–607.
- Pica Ciamarca, M., E. Lippiello, C. Godano, and L. de Arcangelis (2010), Unjamming dynamics: The micromechanics of a seismic fault model, *Phys. Rev. Lett.*, *104*, 238001.
- Place, D., and P. Mora (1999), The lattice solid model to simulate the physics of rocks and earthquakes: Incorporation of friction, *J. Comp. Phys.*, *150*, 332–372.
- Rubinstein, S. M., G. Cohen, and J. Fineberg (2007), Dynamics of precursors to frictional sliding, *Phys. Rev. Lett.*, *98*, 226103.
- Segall, P., A. M. Rubin, A. M. Bradley, and J. R. Rice (2010), Dilatant strengthening as a mechanism for slow slip events, *J. Geophys. Res.*, *115*, B12305, doi:10.1029/2010JB007449.
- Shundyak, K., M. van Hecke, and W. van Saarloos (2007), Force mobilization and generalized isostaticity in jammed packings of frictional grains, *Phys. Rev. E*, *75*(R), 010301.
- Song, Ch., P. Wang, and H. A. Makse (2008), A phase diagram for jammed matter, *Nature*, *453*, 629–632.
- Sykes, L. R., and S. Jaume (1990), Seismic activity on neighboring faults as a long-term precursor to large earthquakes in San Francisco Bay Area, *Nature*, *348*, 595–599.
- Vidale, J. E., and H. Houston (2012), Slow slip: A new kind of earthquake, *Phys. Today*, *65*, 38–43.
- Wang, Y., S. Abe, S. Latham, and P. Mora (2006), Implementation of particle-scale rotation in the 3-D lattice solid model, *Pure Appl. Geophys.*, *163*, 1769–1785.

SUPPLEMENTARY MATERIALS

1 Model description

Figure 1-a of the manuscript illustrates the simulated granular gouge layer. The model consists of three primary layers of particles: a driving block at the top, a granular gouge layer and a substrate block at the bottom. The driving and substrate blocks are used to confine the granular gouge by applying a constant normal force in the Y -direction. The top driving block moves at constant velocity in the positive X -direction and applies a shear force to the granular gouge layer.

Each variable/parameter in our 3D DEM model is expressed in terms of the following basic dimensional units: $L_0 = 150 \mu m$, $t_0 = 1 s$ and $M_0 = 1 kg$, for length, time and mass, respectively. L_0 represents the largest particle radius within the overall DEM model.

The driving and substrate blocks are modeled as a system of spherical bonded particles. The structure of these two blocks allows for dynamic interaction with the granular gouge layer during shearing, analogous to tectonic blocks in a fault system. The driving and substrate blocks consist of two sub-layers. The first sub-layer (top layer - brown colored particles- for the driving block and bottom layer -red colored particles- for the substrate block) consists of a Hexagonal Close Packed (HCP) arrangement of particles with radius L_0 . This layer ensures the flexural rigidity of the driving and substrate blocks, while it is allowing elastic deformation and dynamic interaction. The second sub-layer (roughness layer, dark and light blue colored particles) consists of particles with radii distributed within $[0.3; 1.0]L_0$. These roughness layers are meant to increase the roughness in the interaction of the top monosized HCP layers with the granular gouge layer. The driving and substrate blocks have thickness in Y -direction of approximately $7.0L_0$ ($\frac{Thickness_{roughness\ layer}}{Thickness_{HCP\ layer}} = 0.32$). The particle interaction of both the HCP and roughness layer is modeled by radial springs [Place and Mora(1999), Wang et al.(2006)]. The inter-particle radial force is $F_r = K_r \cdot \Delta r$. Δr is the overlap value of two particles, $\Delta r = (r_1 + r_2) - d$, where d is the distance between the two particles and $(r_1 + r_2)$ is the sum of the two particles radii. The radial compressional/tensional spring stiffness K_r is $2.9775 \cdot 10^7 M_0 \cdot t_0^{-2}$.

The granular gouge layer includes a set of spherical, unbonded particles with radius in the range $[0.35; 0.55]L_0$. Initial thickness of this layer is $6.25L_0$, which is about 7 times the average size of the granular gouge layer particles. This thickness is enough for having jamming/unjamming transition in the layer [Marone et al.(2008)]. The granular gouge layer particles interact with each other and with particles of the driving block/substrate via a repulsive Hookean spring with radial and tangential components that represents normal (to the contact plane) and frictional forces respectively [Place and Mora(1999), Wang et al.(2006)]. The radial component has a spring stiffness $K_r = 5.954 \cdot 10^7$

$M_0 \cdot t_0^{-2}$. The spring stiffness of the tangential component is $K_s = 5.954 \cdot 10^7 M_0 \cdot t_0^{-2}$. The frictional interaction among the granular gouge particles is implemented similarly to the model proposed by [Cundall and Strack(1979)]. The tangential contact force is chosen as the minimum value of $K_s \cdot \Delta s$ and the Coulomb threshold value $\mu \cdot F_r$, at each time step. Δs is the tangential component (to the contact plane) of the particles displacement and μ is the friction coefficient between the two particles surfaces and can be either static, μ_s , or dynamic, μ_d . We chose friction coefficient values of $\mu_s = \mu_d = 0.4$ to produce a macroscopic frictional behavior corresponding to quartz sand aggregates. The frictional interaction between the granular gouge particles and the roughness layers' particles is modeled in the same way with the friction coefficients of $\mu_{static} = \mu_{dynamic} = 0.7$. These values were adjusted based on a parametric study to enhance the stick-slip behavior by increasing the frictional interaction at the interface between the two layers.

The particle assemblies of the roughness layers, as well as of the granular gouge layer were initially generated using a space-filling particle insertion method [Schoepfer et al.(2009)]. The type of packing algorithm and the chosen size range of the granular gouge particles result in a quasi-uniform PSD.

The length of the system in the X direction is $70L_0$, while its thickness in the Z direction is chosen as $5.46L_0$. The Z direction thickness corresponds to three layers of HCP particles (in the Z direction) for the driving block (for brevity referred to as $Z_{dim} = 3d$) and gives space, on average, for 6 particles in the Z direction of the granular gouge layer. To determine the sufficient value of Z_{dim} , we ran simulations with $Z_{dim} = [1, 2, 3, 4, 10]d$, corresponding to on average [2, 4, 6, 8, 19] particles in the Z direction of the granular gouge layer. The initial particle packing of these simulations are shown in fig. 1. The friction coefficient time series of these simulations are presented in fig. 2 and show that for $Z_{dim} > 2$, frictional strength of the layer increases significantly and then essentially saturates. The increase of the friction coefficient for $Z_{dim} > 2$ (or equivalently for average number of granular gouge particles in the Z direction > 4) corresponds to the mobilization of the maximum stable combination of possible force chains (in the Z direction) [Tordesillas et al.(2011)]. Periodic boundary conditions are employed in the X direction and allows to simulate an experiment with larger length. The two lateral sides of the medium in Z direction are bounded by frictionless deformable walls with the same stiffness of the granular gouge layer particles to avoid a rigid wall boundary condition and allow for comparable deformation of walls with the particles in contact with them.

Each simulation run consists of two stages. During the first stage, the consolidation stage, no shear load is imposed and the granular gouge layer is compressed by the vertical displacement of both the driving block and the substrate. The displacement continues until the applied normal stress on the granular gouge layer equals the desired value of $\sigma_n = 40$ MPa. The second stage of each simulation run starts after the consolidation stage and consists in keeping the normal load constant on the driving block while applying a constant velocity of $V_{X,0} = 0.004 \frac{L_0}{t_0}$ to the top particles of the driving block. The imposed velocity introduces a shear load to the granular sys-

tem. A ramp protocol is employed for gradually increasing the shear velocity from 0 to $V_{X,0}$ [Griffa *et al.*(2011), Griffa *et al.*(2012), Griffa *et al.*(2013)]. The confining pressure and shear velocity are found to be among the most important parameters determining the type of dynamical regime of the granular layer [Aharonov and Sparks(1999)]. The confining pressure was chosen based on two reasons: first the confining pressure of 40 MPa leads to a more regular and less random stick-slip behavior; second the chosen confining pressure lies in the range of confining pressures in geological fault settings and experimental setups, which varies between a few to a few hundreds MPa. The shear velocity has been selected after a parametric study to identify the pair values of confining pressure and shear velocity (σ_n - $V_{X,0}$) that lead to stick-slip dynamics.

2 Measure of events size

The distinction between the three types of slip events (*i.e.* large slips, microslips before a large slip and small events –afterslips– that follow a large slip event) is based on the change of kinetic energy in the granular gouge layer during the slip event. The kinetic energy of each j -th particle belonging to the granular gouge layer, K_j , is defined as $K_j = K_j^{trans} + K_j^{rot}$, where K_j^{trans} is the j -th particle translational kinetic energy and K_j^{rot} is its rotational kinetic energy. We define the total kinetic energy for the overall granular gouge layer as $K_{tot} \equiv \sum_{j=1, \dots, M} K_j$, with M the total number of granular gouge layer particles. The potential energy of each i -th contact between two grains belonging to the granular gouge layer, V_i , is defined as $V_i = V_i^{normal} + V_i^{tangential}$, where $V_i^{normal} = \frac{1}{2} \frac{(F_r)^2}{K_r}$ is the i -th contact normal potential energy and $V_i^{tangential} = \frac{1}{2} \frac{(F_s)^2}{K_s}$ is its tangential potential energy. F_r and F_s are the normal (radial) and tangential contact forces. We define the total potential energy for the overall granular gouge layer as $V_{tot} \equiv \sum_{i=1, \dots, N_c} V_i$, with N_c the total number of particles' contact in the granular gouge layer. At the onset of a slip event, the kinetic energy increases sharply from the background level. The largest energy release, which derives from the potential energy stored in particle contacts, occurs at the moment of a slip event

The energy released during a slip event with a length of N time steps of size Δt , is defined as $E = \sum_{i=1}^N (K_{tot} - K_{tot,0}) \cdot \gamma \cdot \Delta t$, where γ is the shear strain rate of the driving block, which is calculated as the temporal derivative of the ratio between the driving block top layer displacement and the granular gouge layer thickness (units s^{-1}). The shear strain rate is nearly constant over the time period of a slip event and is used to obtain the correct units of energy for E after the integration in time.

3 Cross-correlation analysis

We have performed a pairwise sliding window cross-correlation analysis for a time series of the event energy release $E(t)$ and slip event rate, $SER(t)$ for

the total time period, $H = [200; 8000] t_0$. First the $E(t)$ and $SER(t)$ signals are smoothed with a running average of width $0.15 [t_0]$. The cross-correlation analysis is done using a sliding window size of $2.5 [t_0]$ and overlap width of $1.5 [t_0]$. The sliding windows size is several times the average slip event size. After having determined the cross-correlation coefficient $\rho(t)$ as a function of time, we determine for each large slip event the maximum cross-correlation coefficient, ρ_{max} , and the time lag between the instant when the cross-correlation is maximal and the onset of the large slip event, τ_{max} .

Here, we analyze as an example, the cross-correlation in a shorter time period $I = [2000; 3000] t_0$. We show the friction coefficient, μ (fig. 3-a), the slip event rate (SER) (fig. 3-b), and event energy release, E (fig. 3-c) signals. Only large slip events with $E > 3.0 \times 10^{-6} M_0 \cdot L_0^2 \cdot t_0^{-2}$ are considered and cross-correlated with the slip rate. The maximum cross-correlation coefficient, ρ_{max} and time lag, τ_{max} are given in fig. 3-d. The results show a cross-correlation coefficient of $\rho_{max} > 0.9$ for most of the marked events, indicating a strong cross-correlation between the energy release, E and SER . For a majority of these large events, negative time lag values are observed, meaning that the slip event rate increases before the onset of the large slip event.

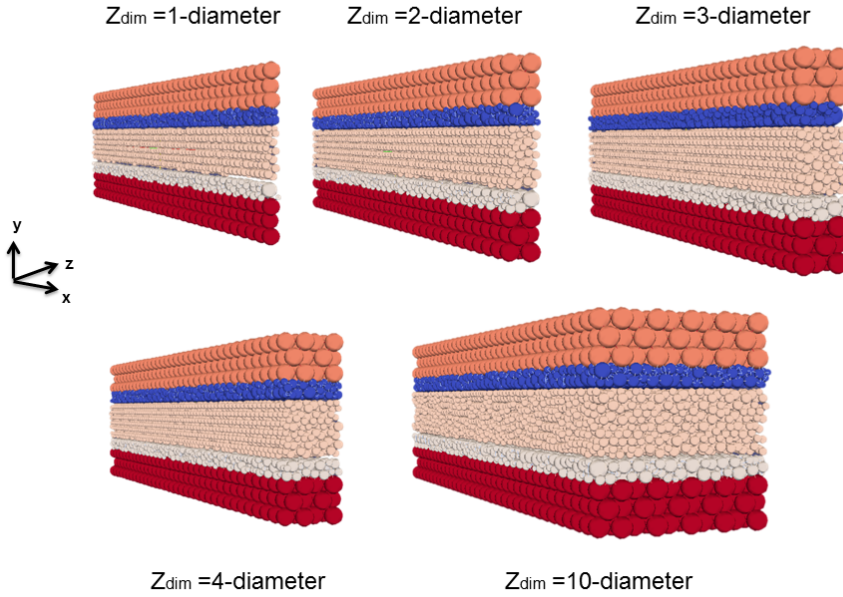


Figure 1: Initial particle packings of simulations with different out of plane (z-direction) widths (bead layers).

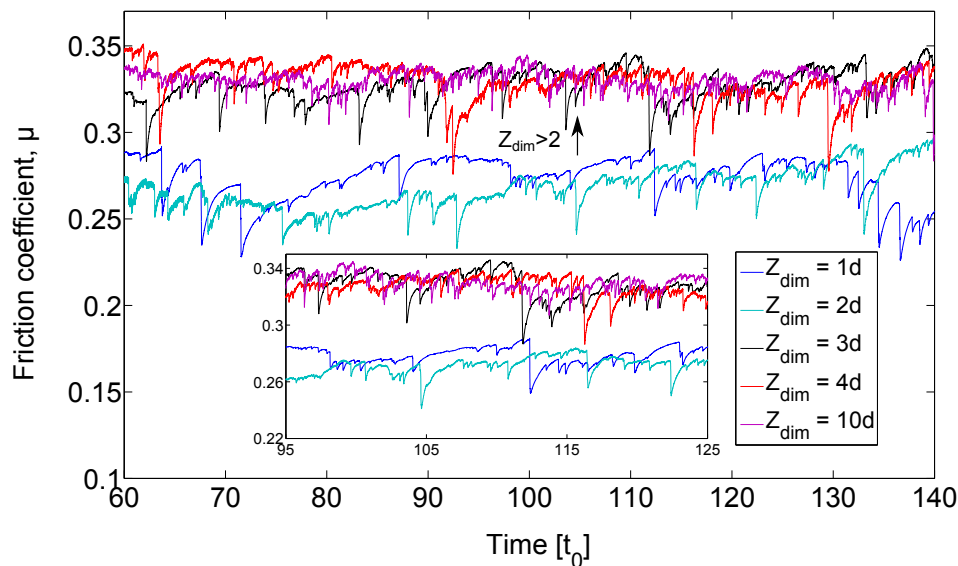


Figure 2: Friction coefficient time series for simulations with different out of plane widths. Inset shows the same time series for time interval $[95; 125]t_0$

References

- [Place and Mora(1999)] Place, D., and P. Mora (1999), The lattice solid model to simulate the physics of rocks and earthquakes: Incorporation of friction, *J. Comp. Phys.* (150), 332-372.
- [Aharonov and Sparks(1999)] Aharonov, E., and D. Sparks (1999), Rigidity phase transition in granular packings, *Phys. Rev. E* (60), 6890-6896.
- [Wang et al.(2006)] Wang, Y., S. Abe, S. Latham, and P. Mora (2006), Implementation of particle-scale rotation in the 3-D lattice solid model, *Pure Appl. Geophys.* (163), 1769-1785.
- [Schoepfer et al.(2009)] Schoepfer, M. P., S. Abe, C. Childs, and J. J. Walsh (2009), The impact of porosity and crack density on the elasticity, strength and friction of cohesive granular materials: Insights from DEM modelling, *Int. J. Rock Mech. Min. Sci.* (46), 250-261.
- [Cundall and Strack(1979)] Cundall, P. A., and O. D. L. Strack (1979), A discrete numerical model for granular assemblies, *Geotechnique* (29), 47-65.
- [Griffa et al.(2011)] Griffa, M., E. G. Daub, R. A. Guyer, P. A. Johnson, C. Marone, and J. Carmeliet (2011), Vibration-induced slip in sheared granular layers and the micromechanics of dynamic earthquake triggering, *Europhys. Lett.* (96), 14001.

- [Griffa et al.(2012)] Griffa, M., B. Ferdowsi, E. G. Daub, R. A. Guyer, P. A. Johnson, C. Marone, and J., Carmeliet (2012), Meso-mechanical analysis of deformation characteristics for dynamically triggered slip in a granular medium, *Philosophical Magazine* (92), 3520-3539.
- [Griffa et al.(2013)] Griffa, M., B. Ferdowsi, E. G. Daub, R. A. Guyer, P. A. Johnson, C. Marone, and J., Carmeliet (2013), Influence of vibration amplitude on dynamic triggering of slip in sheared granular layers, *Physical Review E* (87), 012205.
- [Marone et al.(2008)] Marone, C., B. M. Carpenter, and P., Schiffer (2008), Transition from rolling to jamming in thin granular layers, *Physical Review Letters* (101), 248001.
- [Tordesillas et al.(2011)] Tordesillas, A., Q. Lin, J. Zhang, R. P. Behringer, and J. Shi (2011), Structural stability and jamming of self-organized cluster conformations in dense granular materials, *Journal of the Mechanics and Physics of Solids* (59), 265-296.

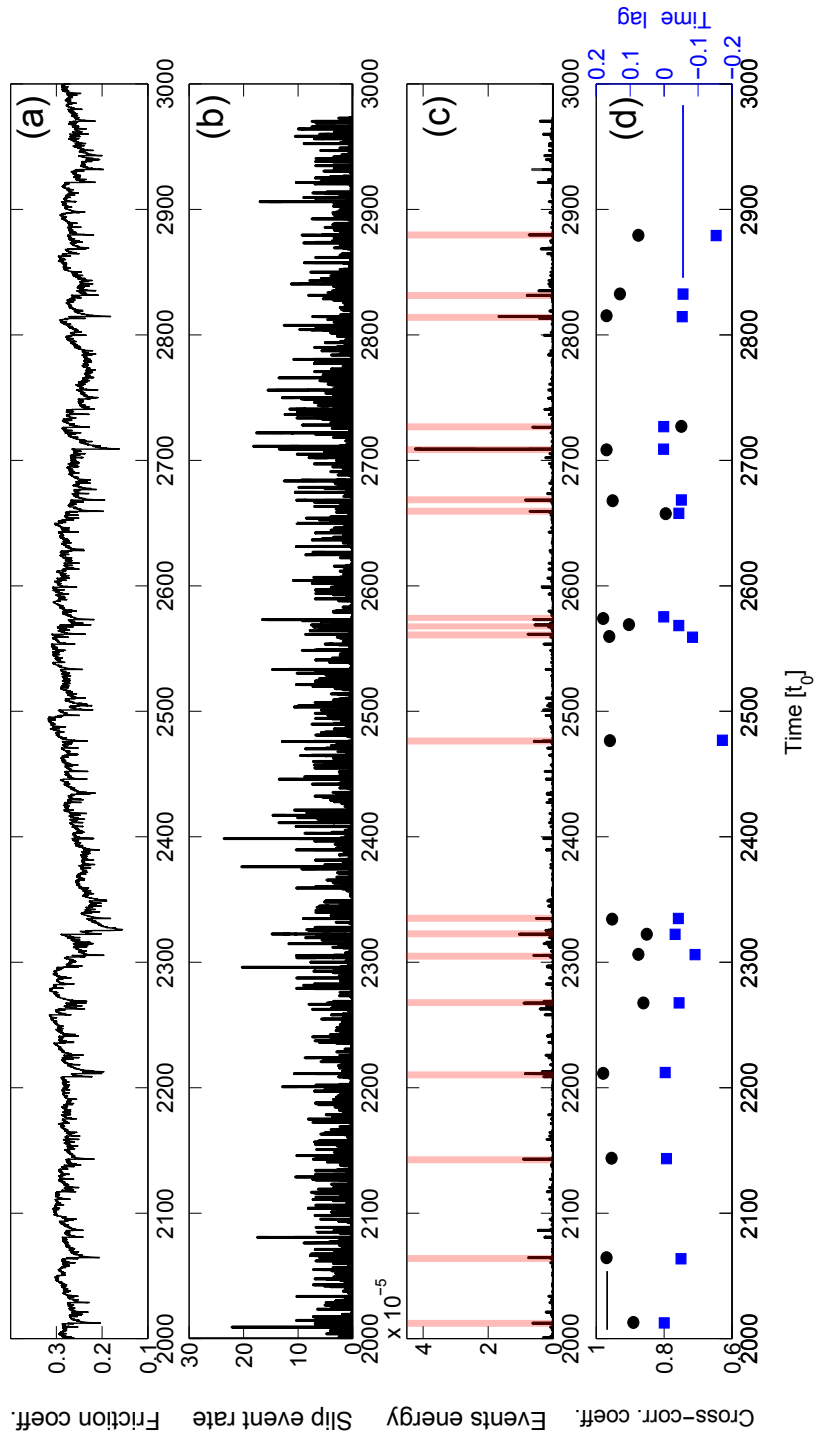


Figure 3: (a) Friction coefficient time series for the time interval $I = [2000; 3000]t_0$. (b) slip event rate time series for the time interval I . (c) Events energy release for the time interval I . Large slip events with $E > 3.0 \times 10^{-6} M_0 \cdot L_0^2 \cdot t_0^{-2}$ are highlighted with a transparent red color box. (d) Cross-correlation results (coefficient and time lag) for those large slip events with $E > 3.0 \times 10^{-6} M_0 \cdot L_0^2 \cdot t_0^{-2}$ within the time interval I .